α–, $\dot{\beta}$–phenomena in the post-symmetry break for the flow past a circular cylinder

Jiten C. Kalita and Shuvam Sen

Citation: Physics of Fluids **29**, 033603 (2017); doi: 10.1063/1.4979065
View online: http://dx.doi.org/10.1063/1.4979065
View Table of Contents: http://aip.scitation.org/toc/phf/29/3
Published by the American Institute of Physics

α-, β-phenomena in the post-symmetry break for the flow past a circular cylinder

Jiten C. Kalita[1,a)] and Shuvam Sen[2,b)]
[1]*Department of Mathematics, Indian Institute of Technology Guwahati, Guwahati 781039, India*
[2]*Department of Mathematical Sciences, Tezpur University, Tezpur 784028, India*

(Received 25 October 2016; accepted 10 March 2017; published online 30 March 2017)

In the existing literature, the so-called α- and β-phenomena have been reported only for the early stages for the flow past an impulsively started circular cylinder. The current study endeavours to explore the possible existence of these phenomena even in the later stages of the flow. The flow is computed using a recently developed compact finite difference method for the biharmonic form of the two-dimensional Navier-Stokes equations for a wide range of Reynolds numbers (Re). We establish that these secondary phenomena not only appear once the wake becomes asymmetric but also periodically during the post-vortex shedding period for $Re = 1000$. Further, the recently reported sub-α- and sub-β-phenomena for $Re = 5000$ at the tertiary level during the early stages of the flow could be identified even during the later stages of the flow as well. The formation of these tertiary structures has been explained through a detailed theoretical characterization of the topological aspects of the boundary layer separation. Both qualitative and quantitative results are provided to substantiate our claim. *Published by AIP Publishing.* [http://dx.doi.org/10.1063/1.4979065]

I. INTRODUCTION

The flow past a circular cylinder problem has been the centerpiece of attraction amongst fluid dynamists over the past century in all the three approaches, namely, experimental, theoretical, and numerical. The prime reason for the huge interest in this flow is the exhibition of a highly complicated and fascinating interplay of primary, secondary, and tertiary vortices along with the phenomenon of vortex shedding in the simplest of geometric settings; the flow characteristics could vary widely over different ranges of Reynolds numbers (Re), thus making the study of this problem even more exciting. Two of such intriguing secondary vortex phenomena are the α- and β-phenomena, which are typical of the flow past an impulsively started circular cylinder in the early stages of the flow.

The α- and β-phenomena have been studied a bit scarcely over the last four decades. Although α-phenomenon can be traced back to the computation of Thoman and Szewczyk[2] in the year 1969, the term was coined by Bouard and Coutanceau in 1980,[1] almost a decade later. In the literature, this secondary phenomenon has been reported at the initial stage of flow with the primary vortex in the wake of the circular cylinder remaining stable. Here streamlines close to the cylinder initially deviate from the surface causing a bulge pattern eventually giving rise to a secondary eddy. This eddy grows in size to such an extent that it touches the boundary of the primary eddy, thereby splitting the primary one into two parts and isolating the region of the wake next to the separation point where another secondary eddy becomes visible. α-phenomenon during the early stages of the flow has been chronicled with great precision in several experimental and numerical works of Bouard and Coutanceau,[1] Loc,[3] and Coutanceau and Defaye.[4] A clear evidence of the α-phenomenon can be seen in Figure 1(a) for $Re = 3000$ at time $t = 2.50$. For higher Re values, another secondary phenomena called β-phenomena precede α-phenomenon. The β-phenomenon, documented both numerically and experimentally in the works of Loc,[3] Loc and Bouard,[5] Chang and Chern,[6] Chou and Huang,[7] Sanyasiraju and Manjula,[8] Kalita and Ray,[9] and Kalita and Sen,[10] emanates with the formation of a very thin recirculating wake. Here the core of the recirculating zone rotates in one piece with a speed which is much faster than the other part of the separated zone forming a vortex which gains strength and size with time. After a while, this vortex separates the initial wake into two parts where the one situated near the point of separation is occupied by two secondary eddies. This phenomenon is clearly exemplified by the flow patterns for $Re = 9500$ at time $t = 1.00$ and is being depicted in Figure 1(b). A complete review of these two secondary phenomena can be found in the work of Kalita and Sen.[11] It is worthwhile to note that the presence of these two phenomena can be found in the whole range $4000 \leq Re \leq 8000$ as evidenced by the work of Kalita and Sen.[11] In Figure 2, we depict the phenomena for two other Reynolds numbers in this range, viz., 4500 and 5500. However, $Re = 5000$ has been a popular choice among the computational fluid dynamics community[8–11] as it exhibits both α- and β-phenomena at certain stages of the early flow evolution for which experimental results are also available.

Kalita and Sen[11] reported the existence of two new tertiary vortex phenomenon for $Re = 5000$ which they termed as sub-α- and sub-β-phenomenon. The sub-β-phenomenon which follow events analogous to β-phenomenon is defined as one where a secondary vortex, part of which is bounded by the free stream, is split by the tertiary vortex and is observed

a)Electronic mail: jiten@iitg.ernet.in
b)Electronic mail: shuvam@tezu.ernet.in

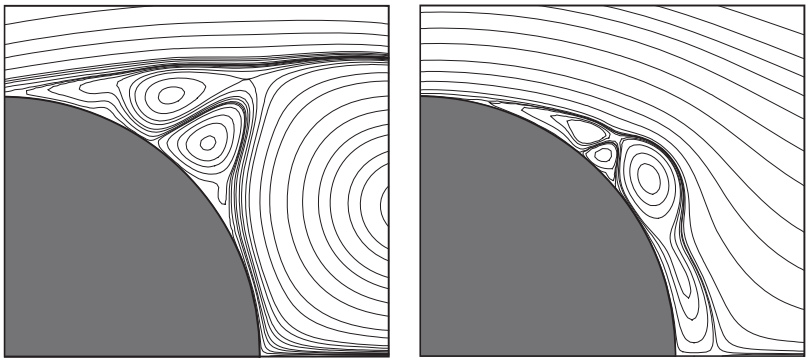

FIG. 1. (a) α-phenomenon for $Re = 3000$ at $t = 2.50$ and (b) β-phenomenon for $Re = 9500$ at $t = 1.00$ form the current computation. The Reynolds number and time are chosen as in the experiments of Bouard and Coutanceau.[1]

with the formation of a tertiary vortex on the surface of the cylinder cushioned by the secondary vortex. The sub-α-phenomenon defined similar to the α-phenomenon where a pair of tertiary vortices is either equivalent in strength or size. Both these phenomena were captured successfully for $Re = 5000$, 8000, 9500, and 10 000 at early times. Along with categorizing this phenomenon in strong and weak sense, they also observed the presence of some α- and β-like phenomena.

For all the secondary and tertiary vortex phenomena described above, their occurrence had been reported only for the early part of the flow beginning from the impulsive start. Even the occurrence of the secondary phenomena, which are quite well reported in the existing literature, has never been reported in the post-symmetry-breaking period. In the present work, we carry out long term simulation and report complete evolution of the flow for $Re = 1000$ and $Re = 5000$ in the post-symmetry break regime. We also record occurrences of sub-α- and sub-β-phenomena at large times for $Re = 5000$ which has not been reported earlier. We demonstrate that these phenomena continue to make their presence even during the vortex shedding period. More interestingly, we observe the periodic occurrence of the α-phenomenon for $Re = 1000$ during the vortex shedding period.

This paper is organized in the following way. In Section II, we briefly discuss the governing equations and the numerical scheme, Section III deals with the observations on the results obtained from our long time simulations for $Re = 1000$ and $Re = 5000$ including a discussion on the underlying mechanism leading to the formation of tertiary vortices, and finally in Section IV, we summarize our achievements.

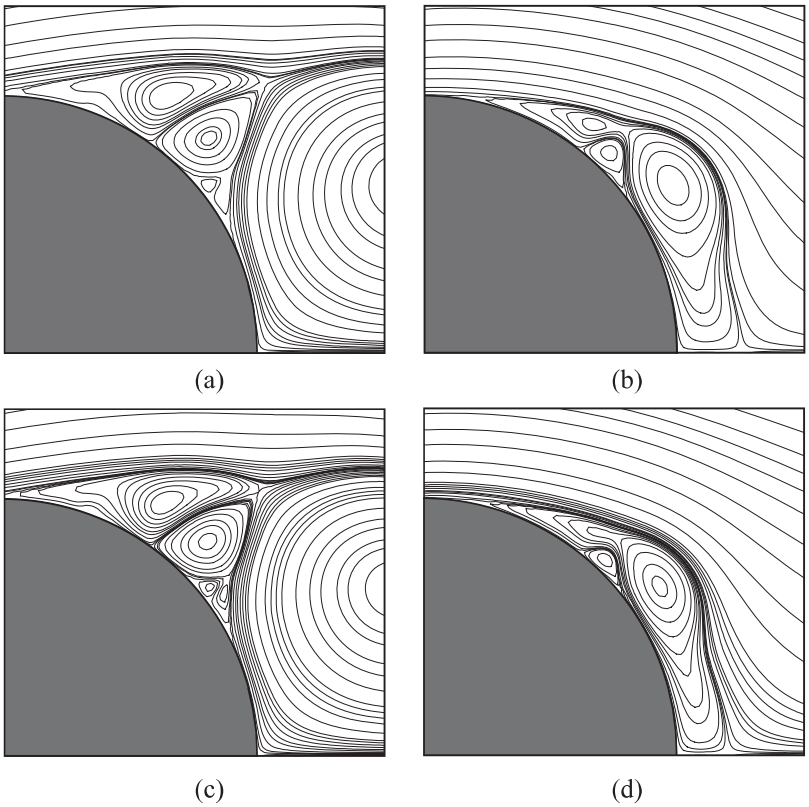

FIG. 2. (a) α-phenomenon for $Re = 4500$ at $t = 2.55$, (b) β-phenomenon for $Re = 4500$ at $t = 1.10$, (c) α-phenomenon for $Re = 5500$ at $t = 2.40$, and (d) β-phenomenon for $Re = 5500$ at $t = 1.00$ form the current computation.

II. THE GOVERNING EQUATION AND ITS DISCRETIZATION

Here, unsteady two-dimensional Navier-Stokes equations are solved using the biharmonic pure stream function formulation following the work of Kalita and Sen.[10,11] The formulation has also been used by the authors with great success in simulating long time flows around various bluff bodies.[12] In the following, we provide a brief outline of the formulation and the numerical scheme used for discretizing the equations governing the flow.

In the Cartesian (x, y) coordinate system, the non-dimensional unsteady pure streamfunction form of Navier-Stokes equations for incompressible flow is

$$\frac{\partial}{\partial t}(\Delta\psi) + [(\nabla^{\perp}\psi).\nabla]\Delta\psi = \frac{1}{Re}\Delta^2\psi. \tag{1}$$

The stream function ψ is related to the velocity field by $(u, v) = \nabla^{\perp}\psi = (\psi_y, -\psi_x)$. We intend to solve the pure stream-function equation in an annular region with inner radius $a = 1$ and outer radius R_∞. This is achieved by converting from the physical (x, y) plane into the computational (ξ, η) plane by using transformation $x + \mathrm{I}y = e^{\pi(\xi+\mathrm{I}\eta)}$, where $\mathrm{I} = \sqrt{-1}$. Following the work of Bouard and Coutanceau,[1] we non-dimensionalise the flow variables as $x = x^*/a$, $y = y^*/a$, $u = u^*/U_\infty$, $v = v^*/U_\infty$, $t = t^*U_\infty/D$, and $Re = DU_\infty/\nu$; u^*, v^* being the dimensional velocities along the x^*-, y^*-directions, respectively, and ν is the kinematic viscosity with $D = 2a$ being the diameter of the cylinder. The semi-discrete second order spatially accurate pure stream-function equation in computational plane can be written as

$$\frac{\partial}{\partial t}\Delta_h\psi_{i,j} = a_{i,j}\Delta_h^2\psi_{i,j} + b_{i,j}\Delta_h\psi_{\xi_{i,j}} + c_{i,j}\Delta_h\psi_{\eta_{i,j}} + d_{i,j}\Delta_h\psi_{i,j}, \tag{2}$$

where

$$a_{i,j} = \frac{4}{\pi^2 e^{2\pi\xi_i} Re}, \qquad b_{i,j} = -\frac{2}{\pi^2 e^{2\pi\xi_i}}\left(\frac{8\pi}{Re} + \psi_{\eta_{i,j}}\right),$$
$$c_{i,j} = \frac{2}{\pi^2 e^{2\pi\xi_i}}\psi_{\xi_{i,j}}, \qquad d_{i,j} = \frac{4}{\pi e^{2\pi\xi_i}}\left(\frac{4\pi}{Re} + \psi_{\eta_{i,j}}\right).$$

The compact discretization operators $\Delta_h^2\psi$ and $\Delta_h\psi$ are defined as

$$\Delta_h^2\psi_{i,j} = \delta_\xi^4\psi_{i,j} + 2\,\delta_\xi^2\delta_\eta^2\psi_{i,j} + \delta_\eta^4\psi_{i,j} + O(h^2), \tag{3}$$

$$\Delta_h\psi_{i,j} = \delta_\xi^2\psi_{i,j} + \delta_\eta^2\psi_{i,j} + O(h^2), \tag{4}$$

with δ_ξ^4 denoting the Stephenson finite difference operator[12]

$$\delta_\xi^4\psi_{i,j} \equiv \frac{12}{h^2}(\delta_\xi\psi_{\xi_{i,j}} - \delta_\xi^2\psi_{i,j}).$$

As noted by Sen *et al.*,[12] we use compatible Padé approximations for ψ_ξ and ψ_η. Finally, Crank-Nicolson time discretization is used to obtain second order temporal accuracy.

The initial and boundary conditions required to compute the flow field are obtained following the work of Kalita and Sen.[11] Although we carried out computations on seven meshes of sizes ranging from 181×301 to 301×1201, unless otherwise stated, the results presented here are with the ones with a grid of size 181×451 and 241×401 where the outer radius R_∞ of the annular computational domain was set as $R_\infty \cong 12$ and $R_\infty \cong 43$, respectively. In case of the former, R_∞ is kept small as we are interested in the flow only in the vicinity of the surface of the cylinder at the earlier stages of the flow, while the latter is specifically chosen for examining the flow in the post-vortex shedding period. Though we computed the flow with time steps varying from 10^{-3} to 10^{-5}, all the subsequent results presented here are from employing a time step $\Delta t = 5 \times 10^{-4}$.

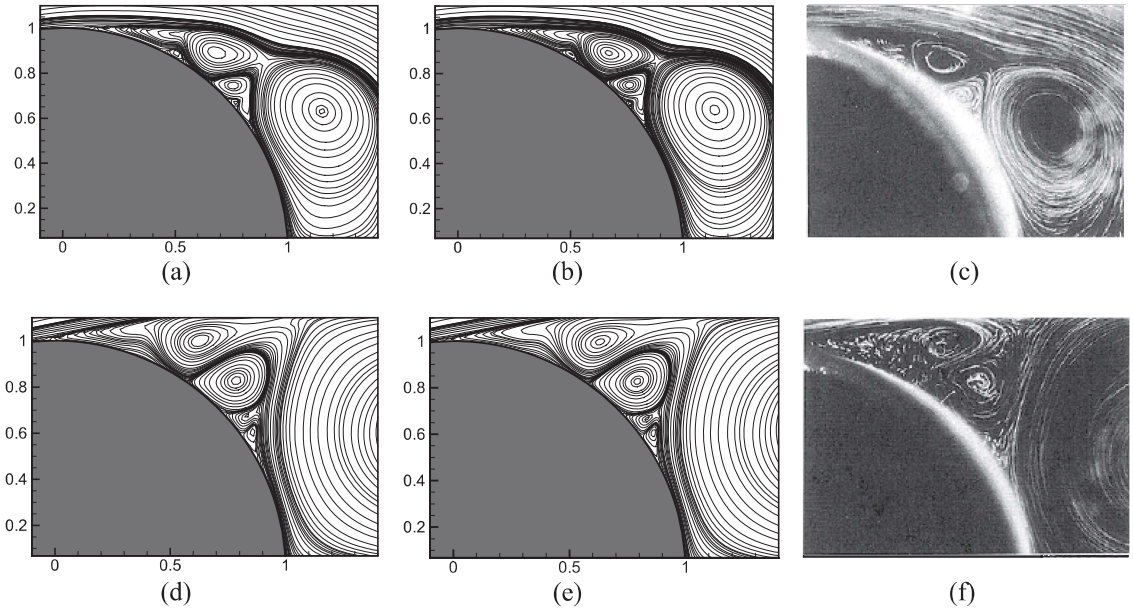

FIG. 3. Comparison of the present simulation with the experimental results of Coutanceau and Defaye[4] for $Re = 4500$: (a) $t = 1.40$ (num. 181×451). (b) $t = 1.40$ (num. 271×676). (c) $t = 1.40$. (Exp., reproduced with permission from M. Coutanceau and J.-R. Defaye, Appl. Mech. Rev. **44**, 255–305 (1991). Copyright 1991 American Society of Mechanical Engineers.) (d) $t = 2.80$ (num. 181×451). (e) $t = 2.80$ (num. 271×676). (f) $t = 2.80$. (Exp., reproduced with permission from M. Coutanceau and J.-R. Defaye, Appl. Mech. Rev. **44**, 255–305 (1991). Copyright 1991 American Society of Mechanical Engineers.)

In order to validate our computed results obtained by using the finite difference scheme described above, we compare our numerical results with some experimental results available in the literature and also perform a grid independence study. In Figure 3, we compare the streamlines obtained through our computation on two different grids of size 181×451 and 271×676 with $R_\infty \cong 12$ at $t = 1.40$ and 2.80 for $Re = 4500$ with the experimental visualization of Coutanceau and Defaye,[4] and one can see that they are very close to each other. This figure also exemplifies the grid independence of our results and better resolution of the tertiary vortices on finer grids.

We also perform an exhaustive grid independence study for both spatial and temporal variations of the grid for $Re = 5000$ when $R_\infty \cong 43$. In Figure 4(a), we plot the time history of drag coefficient C_D till the onset of shedding on four different space grid sizes 181×451, 211×451, 241×401, and 271×451. One can see that the graphs resulting from the last two grids are extremely close to each other. As such, the next study for the temporal grid independence was performed on a spatial grid of size 241×401 by employing the time steps $\Delta t = 0.001$, $\Delta t = 0.0005$, and $\Delta t = 0.000\,125$, respectively. As one can see from Figure 4(b), the graphs of the time history of C_D computed with these time steps are literally indistinguishable from each other indicating the time grid independence of our computed solutions. Further we show the effect of the grid size on the flow characteristics in a tabular form as well. In Table I, we show the separation angle θ_S, the wake length

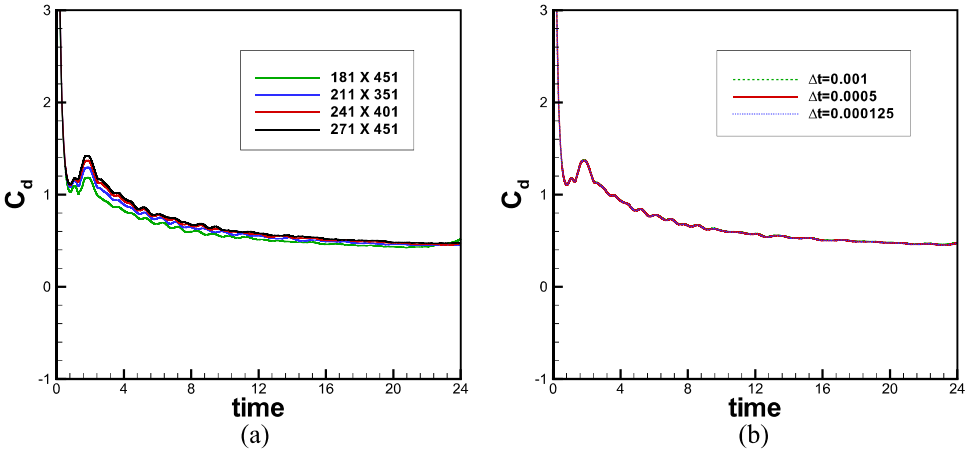

FIG. 4. Grid independence study of time history of drag coefficients for $Re = 5000$ on (a) different space grids and (b) different time grids.

TABLE I. Effect of the mesh size and the outer radius location on flow characteristics for $Re = 5000$ in the upper half of the cylinder.

Mesh		M_1	M_2	M_3	M_4
Grid size		181×451	211×351	241×401	271×451
$R_\infty \cong$		12	43	43	43
$t = 1$	θ_S	80.38	79.34	79.84	80.38
	L	0.216	0.203	0.205	0.207
	C_D	1.181	1.138	1.159	1.159
	$(\bar{x}, \bar{y})$	(0.9484, 0.6498)	(0.9578, 0.6448)	(0.9521, 0.6478)	(0.9378, 0.6373)
$t = 3$	θ_S	94.75	95.73	94.53	95.48
	L	1.672	1.677	1.664	1.668
	C_D	1.129	1.013	1.070	1.102
	$(\bar{x}, \bar{y})$	(1.7539, 0.5834)	(1.7458, 0.5847)	(1.7459, 0.5974)	(1.7548, 0.5702)
$t = 5$	θ_S	97.30	97.88	98.92	98.08
	L	2.411	2.433	2.412	2.419
	C_D	0.900	0.790	0.830	0.850
	$(\bar{x}, \bar{y})$	(1.9488, 0.7716)	(1.9768, 0.7819)	(1.9763, 0.7819)	(1.9454, 0.7702)
$t = 10$	θ_S	100.80	100.52	100.79	100.80
	L	3.664	3.703	3.645	3.611
	C_D	0.659	0.596	0.608	0.612
	$(\bar{x}, \bar{y})$	(2.4288, 0.8843)	(2.3816, 0.8933)	(2.4152, 0.8698)	(2.3825, 0.9042)
$t = 15$	θ_S	101.59	102.88	102.60	102.42
	L	4.255	4.418	4.506	4.448
	C_D	0.590	0.504	0.529	0.538
	$(\bar{x}, \bar{y})$	(2.5558, 0.9713)	(2.6528, 0.9949)	(2.6363, 0.9967)	(2.5403, 1.0049)

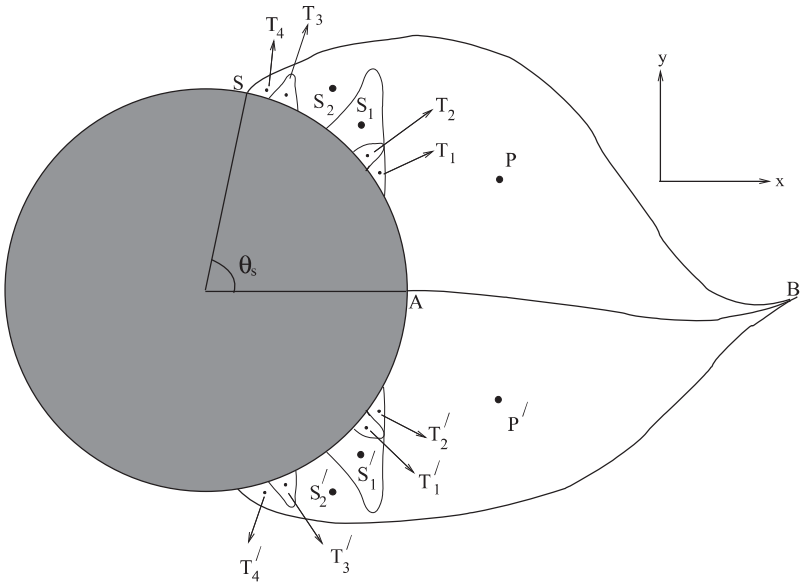

FIG. 5. Schematic diagram of the vortex structures: P, S_i $(1 \le i \le 2)$, T_j $(1 \le j \le 4)$ denote the centers of the primary, secondary, and tertiary vortices, respectively, in the upper half of the cylinder, and the primed letters denote the same in the lower half.

L, and the location of the centre of the upper primary vortex $(\overline{x}, \overline{y})$ at a different time juncture till the onset of asymmetry computed on four grids in the upper half of the cylinder. It is heartening to note that the maximum differences for θ_S, L, and $(\overline{x}, \overline{y})$ values in the last two grids are below 5% for all the flow parameters.

III. RESULTS AND DISCUSSION

A detailed description of the flow past an impulsively started circular cylinder in the pre-symmetry breaking regime can be found in the authors' previous work.[11] The present work is concerned with the post-symmetry breaking period leading to vortex shedding. Maintaining the same convention used by the authors in earlier work[11] for the primary, secondary, and tertiary vortices, we reproduce the schematic diagram of the vortex structures in Figure 5, now at the juncture of onset of asymmetry. Here the rounded structure represents the circular cylinder, S is the point of separation, θ_s is the angle of separation, A is the rear most point on the cylinder, and B is the point on the primary wake farthest from the cylinder. The letters P, P' denote the centers of the primary, S_1,S_2, S_1', S_2', the centers

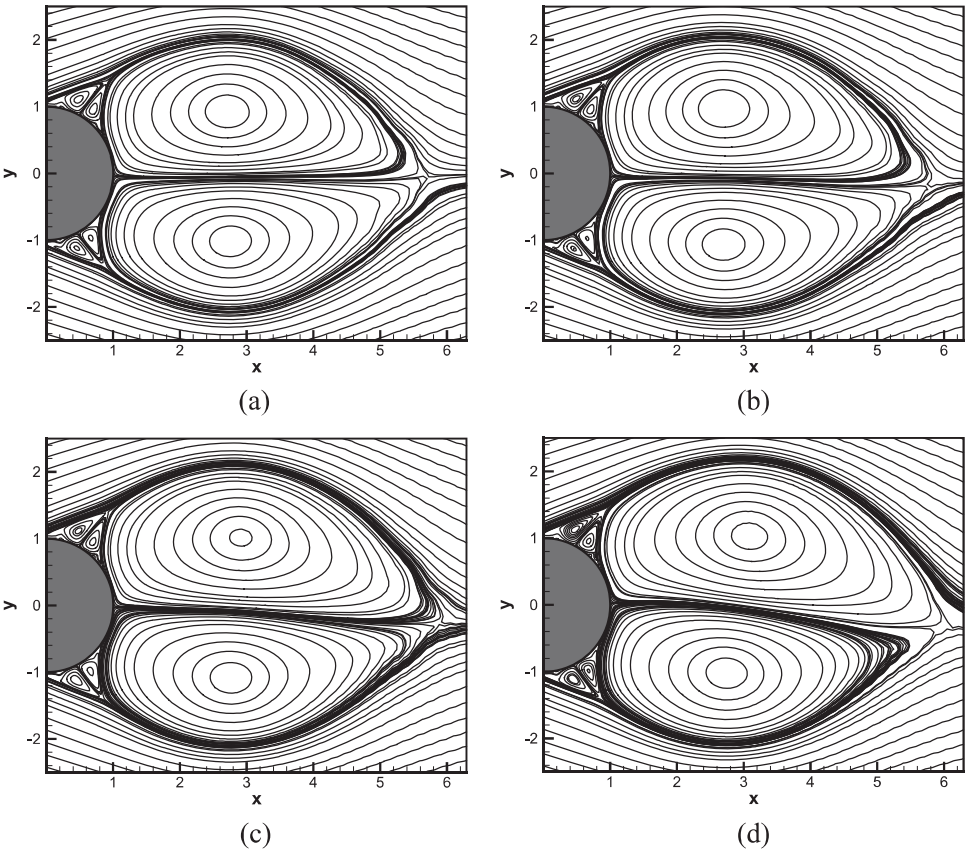

FIG. 6. Onset of asymmetry for the flow past circular cylinder problem for Re = 5000, streamlines at (a) t = 17.00, (b) t = 18.00, (c) t = 19.00, and (d) t = 20.00.

of the secondary, and T_1-T_4, T_1'-T_4', the centers of the tertiary vortices behind the cylinder. The primed letters denote vortices in the lower half of the cylinder while non-primed ones refer to vortices in the upper half. Note that, almost instantly after the impulsive start, the flow separation takes place on the surface of the cylinder and a pair of symmetric vortices grow behind the cylinder. These two primary vortices grow in size and strength with their centers P, P' shifting towards the downstream of the flow. Meanwhile, the interplay amongst the primary, secondary, and tertiary vortices continues on the surface of the cylinder giving rise to the intriguing phenomena, namely, α-, β-, sub-α-, sub-β-, and β-like phenomena. After a while, the symmetry of the flow is broken presaging the onset of vortex shedding.

A. The sub-α-phenomenon preceded by the sub-β-phenomenon

For $Re = 5000$, the upper and lower primary vortices lose their symmetry about the x-axis at the tail of the wake around time $t = 18.00$ and the break in the symmetry becomes completely obvious at $t = 20.00$. We depict the onset of asymmetry of the wake in Figure 6. Prior to this, the secondary and tertiary vortex phenomena take place at the early stages of the flow. It is well known that for $Re = 5000$, the α-phenomenon is preceded by the β-phenomenon. Likewise, it was found by Kalita and Sen[11] that at times the sub-α-phenomenon is preceded by the sub-β-phenomenon in early stages of the flow when the flow is still symmetric about the x-axis. We now show that such phenomena occur even after the symmetry in the flow is broken. However, the duration of such an occurrence is very short. The first of this occurs when the tertiary vortex $\mathbf{T}_3$ reappears at around $t = 22.60$ on the upper half surface and becomes clearly visible at $t = 22.85$ as can be seen from Figures 7(a)–7(b). It grows in size and strength and splits the secondary vortex $\mathbf{S}_2$ into two parts $\mathbf{T}_3$ and $\mathbf{T}_4$ (Figures 5 and 7(c)–7(e)) leading to the formation of a pair of tertiary vortices (Figure 7(f), $t = 23.40$: ψ values at the centers are –0.000 642 3 and 0.000 440 5). However, they are quickly washed away by the free-stream just on the eve of the vortex shedding process.

A similar event can be seen at the lower half of the cylinder as well which last almost three times in duration than the one at the upper half described above. Here the tertiary vortex $\mathbf{T}'_3$ surrounded by $\mathbf{S}'_2$ reappears at around $t = 20.00$ and the pair of tertiary vortices $\mathbf{T}'_3$ and $\mathbf{T}'_4$ (Figure 5) forming the sub-α-phenomenon is closest to each other in strength at $t = 25.00$ with ψ values –0.004 125 7 and 0.003 869 4 at their centers. The sequence of events can be seen in Figures 8(a)–8(d). Gradually, the tertiary vortices lose their strengths, merge with one another somewhere around $t = 26.00$, and eventually are swept away by the free stream.

The evidence of the sub-α-phenomenon preceded by the sub-β-phenomenon will also be observed in the post-vortex shedding period in Sec. III B.

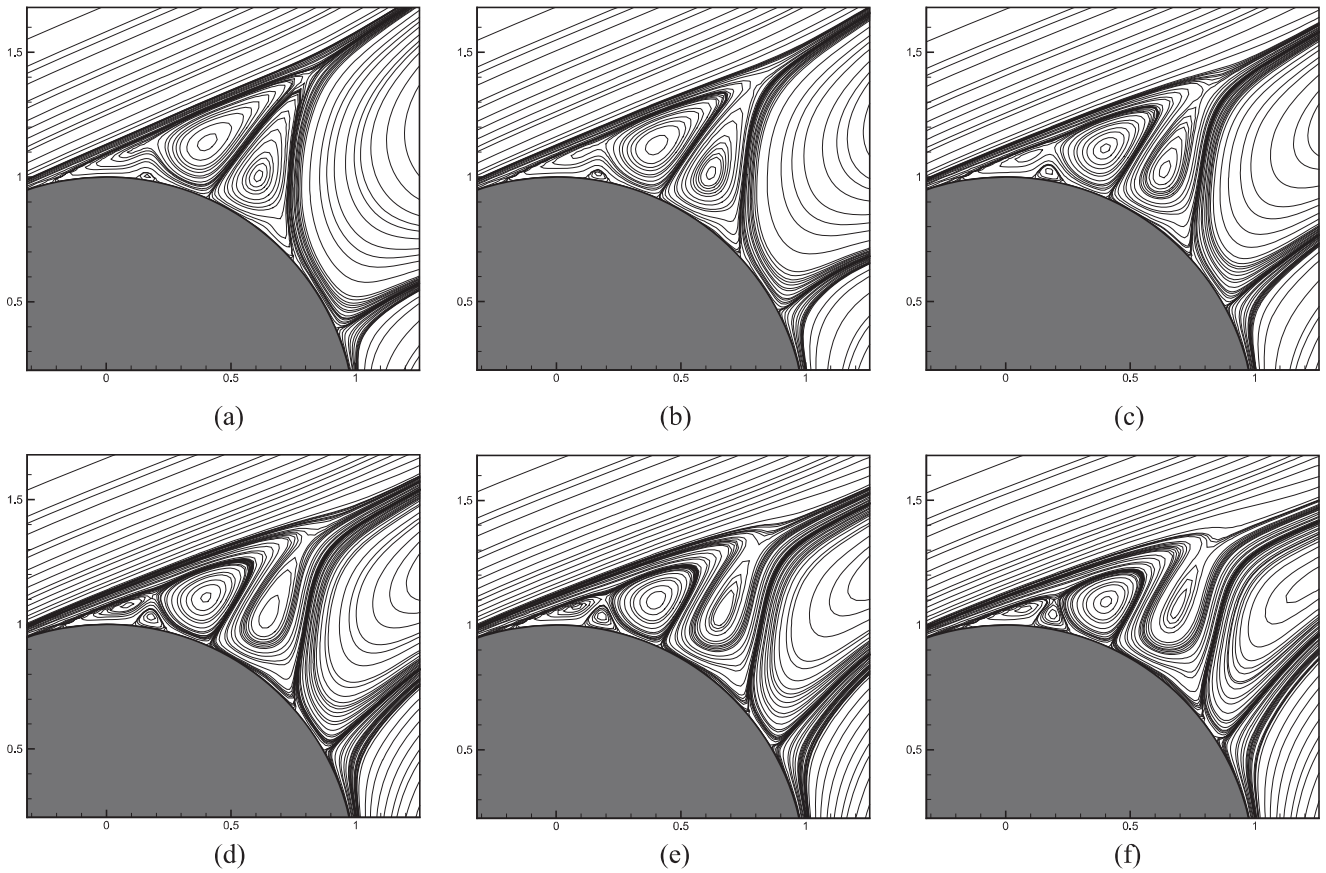

FIG. 7. The sub-β-phenomenon followed by the sub-α-phenomenon, streamlines in the upper half: (a) $t = 22.60$, (b) $t = 22.85$, (c) $t = 23.10$, (d) $t = 23.20$, (e) $t = 23.30$, and (f) $t = 23.40$ for $Re = 5000$.

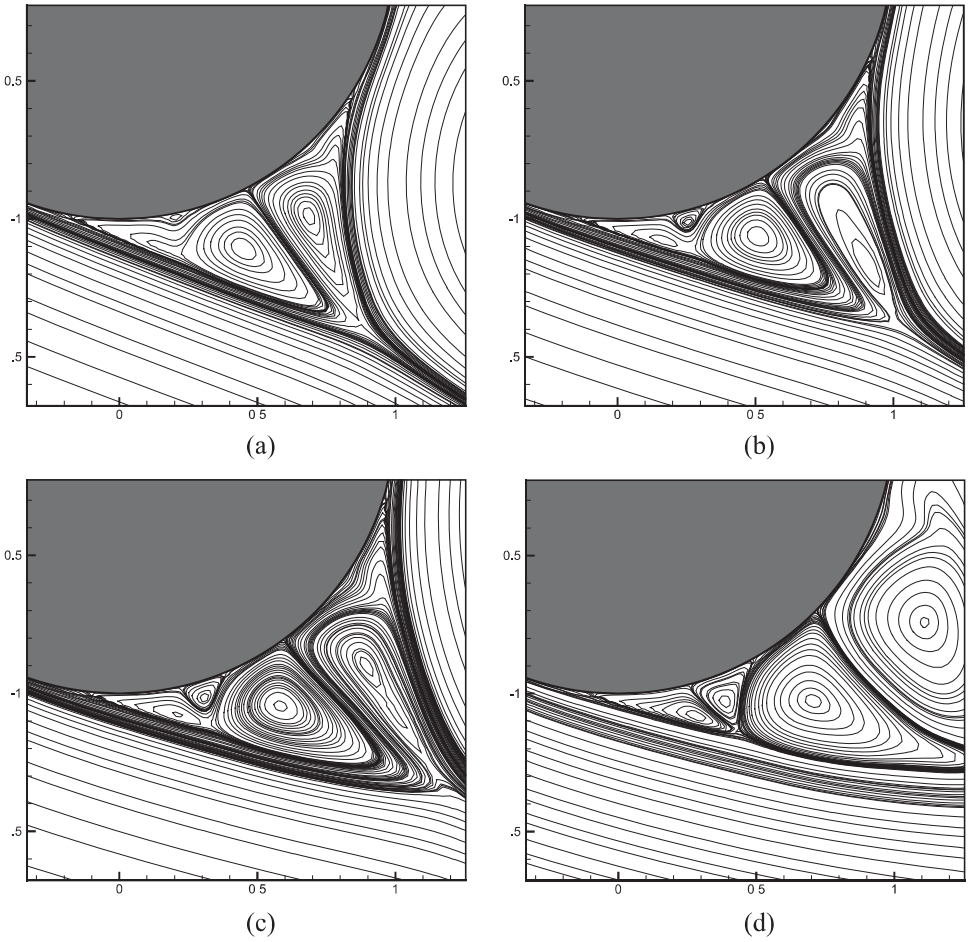

FIG. 8. The sub-β-phenomenon followed by the sub-α-phenomenon, streamlines in the lower half: (a) t = 20.25, (b) t = 22.00, (c) t = 23.00, and (d) t = 25.00 for Re = 5000.

B. Post-vortex shedding secondary and tertiary phenomena

Long time flow computations on the impulsively started circular cylinder by Thoman and Szewczyk[2] and Chou and Huang[7] indicate the occurrence of vortex shedding for Reynolds number as high as 40 000. It will be interesting to see whether the secondary and tertiary vortex phenomena described in Sec. III A still persist in the post-shedding regime as well and if so, whether the event is periodic or not. In order to check this, at first, we probe the flow for Re = 1000. As in the work of Chou and Huang,[7] we also found the flow to be periodic in the post-vortex shedding regime; in Figure 9 and Table II, we present our results for a complete periodic cycle over five successive instants of time. In this sequence, Figures 9(a) and 9(c); 9(c) and 9(e); and 9(b) and 9(d) are half a vortex shedding cycle apart and each of these combinations is a mirror image of the other. Figures 9(a) (also 9(e)) and 9(c) are indicative of the presence of a "pair of secondary vortex" constituting the α-phenomenon at the top and bottom surfaces respectively during these instants of time. This is further confirmed by Table II where we have tabulated the strength of the primary and secondary vortices over those instants. The extreme closeness of the strengths of $\mathbf{S}_1$ and $\mathbf{S}_2$ at times $t = T$ and $t = T + T_0$ and the strengths of $\mathbf{S'}_1$ and $\mathbf{S'}_2$ at time $t = T + \frac{T_0}{2}$ is clear evidence of α-phenomenon during those instants.

Further, we see that the magnitudes and the signs of the values of $(\mathbf{P}, \mathbf{P}, \mathbf{P})$ and $(\mathbf{S}'_2, \mathbf{S}_2, \mathbf{S}'_2)$ at $(T, T + \frac{T_0}{2}, T + T_0)$, and $(\mathbf{P}, \mathbf{P})$ and $(\mathbf{S}_1, \mathbf{S}'_1)$ at $(T + \frac{T_0}{4}, T + \frac{3T_0}{4})$ assert the periodicity of the flow, and also the fact at half a period apart, the streamlines (as well as vorticity contours, not shown here) are mirror images of each other. Here T denotes a particular instant of time after periodic shedding and T_0 is the period of one vortex shedding cycle. It is interesting to note that while α-phenomenon was completely absent in the strong sense in the early stages of the flow, it can be found in the post-shedding period for this Re.

Next, we move our attention towards the post-vortex shedding period for Re = 5000. Note that the cycles of vortex shedding are not exactly periodic for this Reynolds number and as such it is not possible to get mirror images like Figure 9. However, even during the post-shedding period, the flow is replete with the presence of α-phenomenon, sub-α-phenomenon in isolation, and sub-α-phenomenon preceded by sub-β-phenomenon. In Figure 10(a), we depict the sub-α-phenomenon in isolation in the lower half of the cylinder at t = 35.74 while the events leading to sub-α-phenomenon preceded by sub-β-phenomenon in the upper half of the cylinder are presented in Figures 11(a)–11(c) (also see Figure 10(b)). In Figure 11(d), we depict the α-phenomenon which occur shortly after at time t = 42.15. The strengths of the secondary and tertiary vortices corresponding to these events

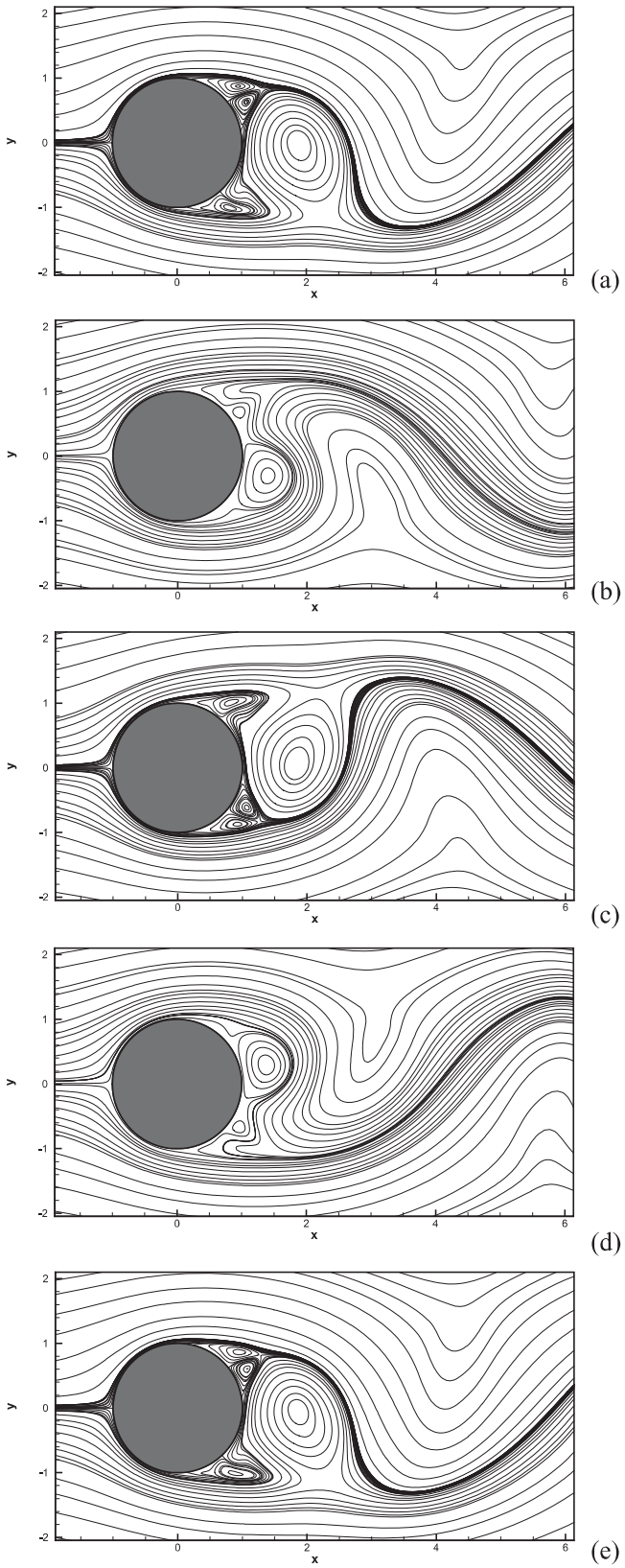

FIG. 9. The streamfunction contours depicting the wake behind the cylinder for $Re = 1000$ for five successive instants of time (a) $t = T$, (b) $t = T + \frac{T_0}{4}$, (c) $t = T + \frac{T_0}{2}$, (d) $t = T + \frac{3T_0}{4}$, (e) $t = T + T_0$.

are presented in Table III. These figures are also indicative of the pace at which the secondary and tertiary vortices are formed.

C. Unsteady flow separation in the post-symmetry break regime

Earlier studies by the authors (Kalita and Sen[11]) and Figures 6(a)–6(d) reveal that the α-phenomenon continues to persist even after the symmetry in the flow is broken. However, the occurrence of the sub-α- and sub-β-phenomenon which is typical of tertiary vortex dynamics in the post-symmetry breaking and post-shedding period is a new observation. Juxtaposed to the longer duration of the secondary vortex phenomena, one can observe intermittent appearance and disappearance and sometimes persistent stay of tertiary vortices around a particular location without leading to the sub-α- and sub-β-phenomenon. The underlying mechanism behind the formation of these structures before the symmetry break during the early stages of the flow has already been described by the authors.[11] In this section, we shall illustrate one of the many such tertiary vortex phenomena after the symmetry break by the structural bifurcation theory proposed by Ma and Wang[13] and Ghil *et al.*[14,15] and also the viscous-inviscid interaction of unsteady boundary layer separation induced by a vortex by Obabko and Cassel.[16,17]

The formation of the primary secondary and tertiary vortices, which gives way to multiple separation zones on the surface of the cylinder in the early stages of the flow, can also be seen in the post-symmetry break period. For complete understanding of the interplay of these vortices, one needs to carefully examine the vorticity distribution on the surface of the cylinder. The extent and size of these vortices can be gauged by the alternate positive and negative values of vorticity on the surface of the cylinder. In Figure 12(a), we show several recirculation zones on the surface of the cylinder by plotting the streamlines over the whole cylinder just before the onset of sub-α-phenomenon on the lower half of the cylinder preceded by the sub-β-phenomenon at $t = 23.20$. The corresponding vorticity distribution on the surface of the cylinder at the same instant of time is shown in Figure 12(b). The separation points and the recirculation zones enclosed by a pair of such points have been indicated by marking them with numbers 1-13. This figure clearly demonstrates the one to one correspondence between the recirculation zones and vorticity distribution which will be used in the subsequent discussion to delve more into the making up of these vortices.

The boundary layer separation theory proposed by Ghil *et al.*[14,15] also uses vorticity as a tool to predict the location and time of the formation of a recirculation zone. The conditions for the separation of flow on the surface of a wall are given as follows:

$$\omega(P,T) = 0, \quad \frac{\partial \omega}{\partial \tau} = 0, \quad \frac{\partial^2 \omega}{\partial \tau^2} > 0, \quad \frac{\partial \omega}{\partial t} < 0, \tag{5}$$

where ω is the vorticity, t the time, and τ is the direction tangential to the wall. It is assumed that structural bifurcation occurs at time T and the normal derivative of the velocity field $\frac{\partial \mathbf{u}}{\partial n}$ ($\mathbf{u} = (u, v)$ is the velocity field and n is the direction normal to the wall) has a degenerate singular point P on the wall; it is also assumed that on the wall, no slip boundary conditions are imposed and the shear flow is downward. When the flow is upward, the last two inequalities in Equation (5) undergo change of signs.

TABLE II. Strengths of primary and secondary vortices during the vortex shedding period for Re = 1000 corresponding to Figure 9.

	Vortices				
Time	**P**	$\mathbf{S}_1$	$\mathbf{S}_2$	$\mathbf{S'}_1$	$\mathbf{S'}_2$
$t = T$	−0.589 1259	0.028 989 4	−0.029 043 6	...	0.011 569 2
$t = T + \frac{T_0}{4}$	0.193 834 2	0.015 063 9	...	...	...
$t = T + \frac{T_0}{2}$	0.571 003 3	...	−0.015 594 1	−0.030 210 8	0.029 752 8
$t = T + \frac{3T_0}{4}$	−0.189 872 1	...	...	−0.016 458 9	...
$t = T + T_0$	−0.579 389 2	0.027 626 7	−0.027 493 2	...	0.016 660 9

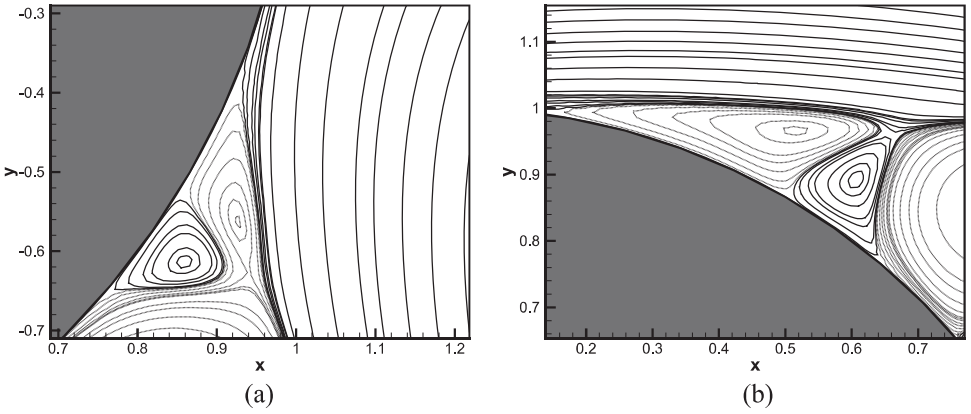

FIG. 10. Streamfunction contours representing the sub-α-phenomenon at (a) t = 35.74 and (b) t = 42.03 for Re = 5000 (solid lines for positive and dotted lines for negative values, grid size: 481×801).

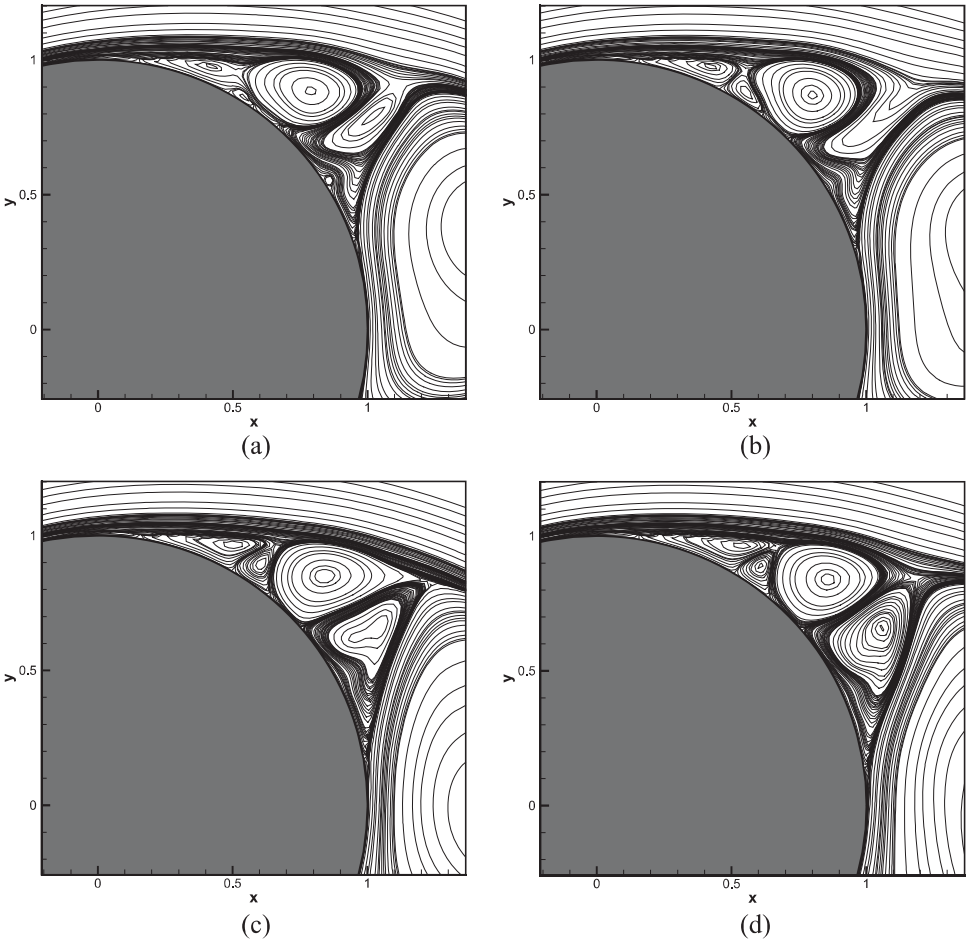

FIG. 11. The post-shedding period, the sub-β-phenomenon followed by the sub-α-phenomenon, streamlines in the upper half: (a) t = 41.615, (b) t = 41.70, and (c) t = 42.00; the α-phenomenon at (d) t = 42.15 for Re = 5000.

TABLE III. Strengths of secondary and tertiary vortices during the vortex shedding period for $Re = 5000$.

	Vortices					
Time	$\mathbf{S}_1$	$\mathbf{S}_2$	$\mathbf{T}_3$	$\mathbf{T}_4$	$\mathbf{T'}_1$	$\mathbf{T'}_2$
$t = 35.74$ (Figure 10(a))	...	...	...	...	−0.001 651 9	0.001 664 5
$t = 42.03$ (Figure 10(b))	...	...	0.002 9567	−0.002 939 2	...	...
$t = 42.15$ (Figure 11(d))	0.062 850 9	−0.061 122 8	...	...	...	...

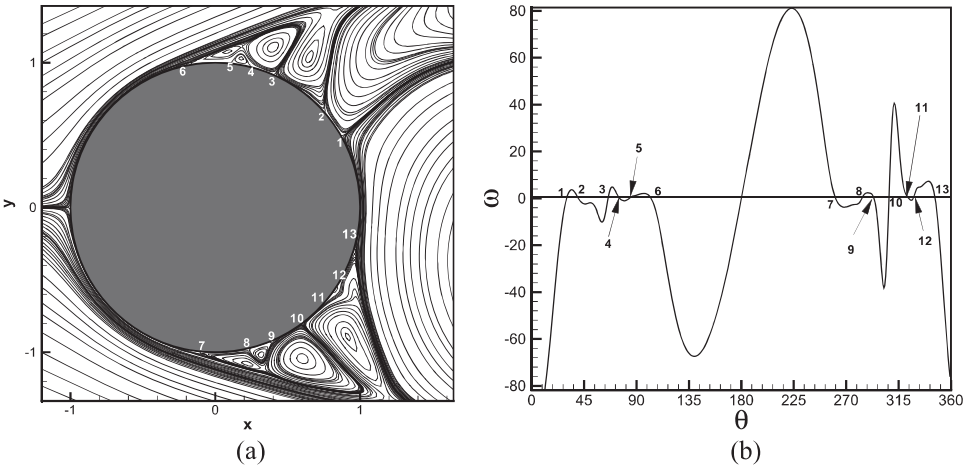

FIG. 12. (a) Recirculation zones depicted by streamlines and (b) vorticity distribution on the surface of the cylinder at $t = 23.20$ for $Re = 5000$ on grid size 361×901.

Note that during the early stages of the flow, tertiary vortices responsible for the sub-α- and sub-β-phenomenon, immediately after inception, grow in strength and size to split the secondary vortices cushioning them eventually leading to the sub-α-phenomenon. However, the tertiary vortices causing these phenomena after symmetry break lack the strength required to grow in size, and as such sits in the same location for quite some time. For example, the tertiary vortices between the pairs of points (4, 5) and (8, 9) in Figure 12 in the upper and lower halves of the cylinder, respectively, had their inception much before the symmetry break at a very early stage around $t = 2.00$. They alternate between growing and shrinking slenderly in size and shifting their centers in small neighbourhoods eventually making the final push at around $t = 22.00$ to split the secondary vortices (lying between the pair of points (3, 6) and (7, 10) in Figure 12) leading to the sub-α- and sub-β-phenomenon.

Authors in their earlier work[11] discussed structural bifurcation and unsteady flow separation in the very early stages of the flow when the flow is essentially symmetric and as such the upper half was a true representation of the whole cylinder for explaining the tertiary vortex dynamics. Here we have chosen the lower half of the cylinder to explain the formation of one of the tertiary vortices after the symmetry break around time $t = 23.20$. In Figures 13(a) and 13(b), we show the close up view of the streamfunction contours at $t = 22.82$ and $t = 23.40$, respectively, on the lower half of the cylinder. In Figure 13(a), one can clearly see the trace of a tertiary vortex between points 11 and 12 in the vicinity of $\theta = 324.8°$ (refer to Figure 12(b) as well), which is more evident in Figure 13(b). This is corroborated by Figure 14(a), which shows the surface vorticity distribution on the lower half of the cylinder at the same time junctures and suggests that the birth of this vortex actually takes place sometimes between $t = 22.82$ and $t = 23.40$.

The primary and secondary vortices are formed behind the cylinder much earlier; details of it can be found in the authors' work.[11] The primary vortices produce adverse pressure gradients leading to the formation of secondary vortices,

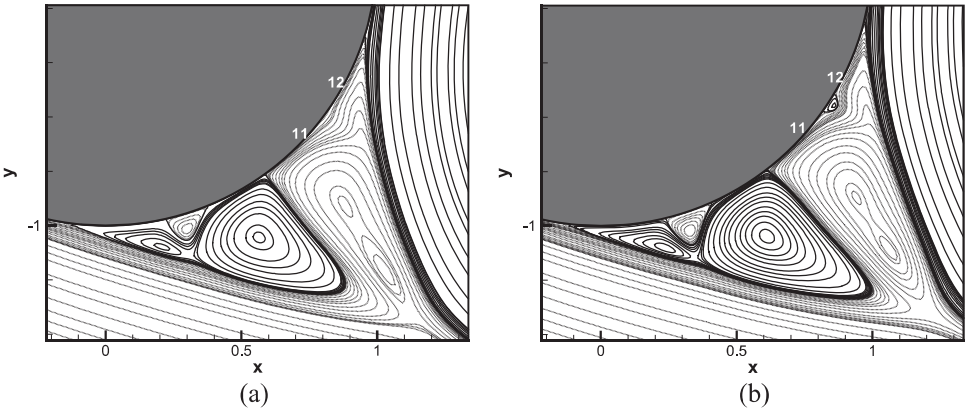

FIG. 13. Close up view of the streamfunction contours on the lower half of the cylinder at (a) $t = 22.82$ and (b) $t = 23.40$ for $Re = 5000$ on grid size 361×901.

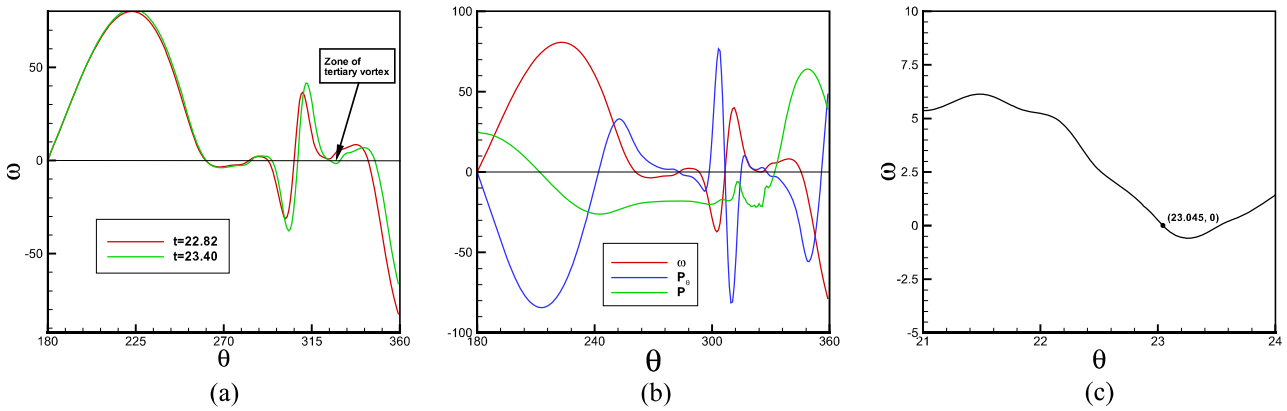

FIG. 14. (a) Vorticity distribution just before and after the formation of the tertiary vortex and (b) distribution of vorticity, pressure, and pressure gradient at t = 23.045 on the surface of the cylinder in the lower half and (c) time history of vorticity at the point $\theta = 324.8°$ for $Re = 5000$.

which in turn produce adverse pressure gradients in the opposite direction of the previous one eventually resulting in the formation of tertiary vortices. In Figure 14(b), we show the distribution of vorticity ω (which is scaled down in order to make it comparable with pressure and pressure gradient), the pressure p and $\frac{\partial p}{\partial \theta}$ along the surface of the cylinder at time t = 23.045. It is clear from Figure 12(b) that the vorticity value reaches zero at $(\theta, t) = (324.8°, 23.045)$ as a local minimum in space and decreases in time, that is, $\omega(324.8°, 23.045) = 0$, $\frac{\partial \omega}{\partial \theta}(324.8°, 23.045) = 0$, $\frac{\partial^2 \omega}{\partial \theta^2}(324.8°, 23.045) > 0$. In Figure 14(c), we show the time history of the vorticity value at the point $\theta = 324.8°$ on the surface; this figure clearly shows that $\frac{\partial \omega}{\partial t}(324.8°, 23.045) < 0$. Thus all the conditions given by Equation (5) are satisfied confirming the occurrence of a structural bifurcation at time t = 23.045 at $\theta = 324.8°$ on the surface of the cylinder.

In Figures 15(a) and 15(b), we show the combined streamfunction and vorticity contours in the neighborhood of the point $\theta = 324.8°$ in the θ-r plane at the same time junctures discussed above. Here the r scale has been magnified 10 times in order to have a better view. These figures will help us explain the formation of this vortex in the light of the theory of viscous-inviscid interaction of unsteady boundary layer separation induced by a vortex by Obabko and Cassel.[16,17] The secondary vortex lying between the points 10 and 13 on the surface of the cylinder in Figure 12 produces an adverse pressure gradient. Just before the formation of the tertiary vortex (refer to Figures 13(a) and 15(a)), the pressure gradient

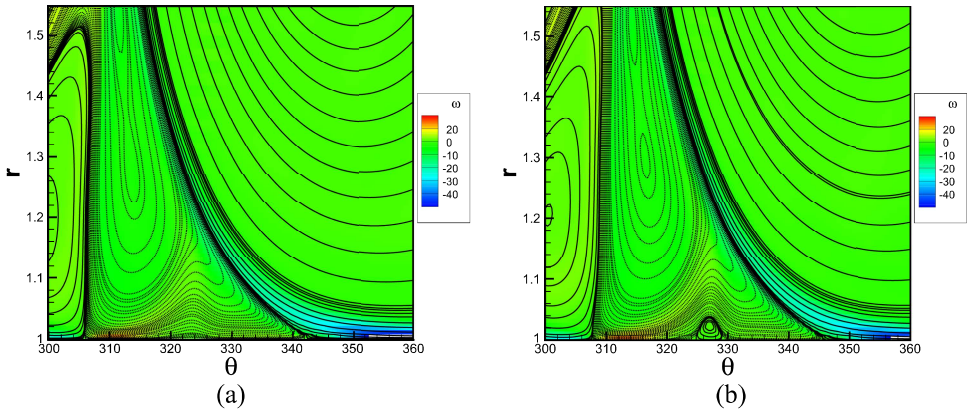

FIG. 15. Combined streamfunction and vorticity contours for Re = 5000 at (a) t = 22.82 and (b) t = 23.40. (Streamfunction with line option and vorticity contours with flood option. The solid lines for positive and dotted lines for negative streamfunction values, grid size: 361 × 901.).

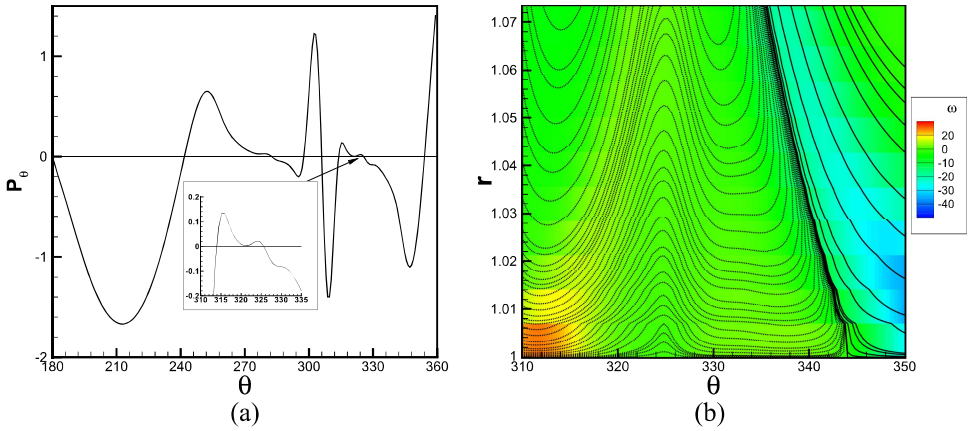

FIG. 16. (a) Distribution of surface pressure gradient at t = 22.82 on the lower half of the cylinder and (b) combined streamfunction and vorticity contours at t = 23.04 for Re = 5000. (Streamfunction with line option and vorticity contours with flood option. The solid lines for positive and dotted lines for negative streamfunction values, grid size: 361 × 901.).

begins changing in the vicinity of its minimum exactly where the structural bifurcation takes place eventually. As one can clearly see in Figure 16(a) which depicts the distribution of surface pressure gradient on the lower half of the cylinder at $t = 22.82$, there is a presence of a local minimum for p_θ at $\theta \cong 324.8°$. This local minimum having a positive value becomes locally adverse immediately afterwards attaining a negative value leading to the formation of the tertiary vortex in Figures 13(b) and 15(b).

In Figure 16(b), we again show the close up view of the streamfunction contours at time $t = 23.04$ in the θ-r plane where the scales have been further magnified to show the flow pattern more clearly within the boundary layer which is of the order $Re^{-\frac{1}{2}}$. Note that, in the later stages, after the formation of the secondary vortex represented by the zone between the points 10 and 13 in Figure 12, the boundary layer concentrates on a narrow region that forms on the upstream side of the recirculation zone. Since the fluid particle at the separation point is rapidly compressed in the streamwise direction, it elongates in the direction normal to the wall. The elongation of the fluid particle in the normal direction leads to the growth of a sharp spike (Obabko and Cassel,[16] Obabko and Cassel,[17] Cassel *et al.*[18]) leading to what is called as the spike formation just before the formation of tertiary vortex. This spike is clearly visible from our computation as can be seen at time $t = 23.04$ in Figure 16(b), thus validating the birth of the tertiary vortex at time $t = 23.045$ discussed above.

IV. CONCLUSION

In this study, we make some interesting observations on the flow phenomena that can be observed during α- and β-phenomena which are typical of the flow past of an impulsively started circular cylinder at moderately high Reynolds numbers by numerically solving the biharmonic pure streamfunction form of the Navier-Stokes equations. Contrary to the belief that these phenomena occur at the very early stage of the flow, we have shown that they are very much in existent even during the post-shedding period. The evidence of their existence is substantiated by the strengths of the secondary vortices forming such phenomena at later stages of the flow. Events similar to the α- and β-phenomena were also observed at the tertiary level in either half of the cylinder once the symmetry of the flow was broken. We have also carried out a detailed analysis on the topological structures of the tertiary recirculation zones using the boundary layer separation theory based on the structural bifurcation concept. This has been further strengthened by explaining the birth of the tertiary structures from the angle of viscous-inviscid interaction. To the best of our knowledge, no report on the existence and quantification of these phenomena is seen in the available literature and our observations may lead to providing more insights into the secondary and tertiary vortex dynamics for flow past bluff bodies other than the circular cylinder.

ACKNOWLEDGMENTS

The second author gratefully acknowledges use of facilities available at the High Performance Computing Centre of Tezpur University sponsored by DeitY, India in collaboration with C-DAC, Pune, India, for carrying out a part of computation.

[1]R. Bouard and M. Coutanceau, "The early stage of development of the wake behind an impulsively started cylinder for $40 \le Re \le 10^4$," J. Fluid Mech. **101**, 583–607 (1980).
[2]D. C. Thoman and A. A. Szewczyk, "Time-dependent viscous flow over a circular cylinder," Phys. Fluids **12**, II-76–II-86 (1969).
[3]T. P. Loc, "Numerical analysis of unsteady secondary vortices generated by an impulsively started circular cylinder," J. Fluid Mech. **100**, 111–128 (1980).
[4]M. Coutanceau and J.-R. Defaye, "Circular cylinder wake configurations: A flow visualization survey," Appl. Mech. Rev. **44**, 255–305 (1991).
[5]T. P. Loc and R. Bouard, "Numerical solution of the early stage of the unsteady viscous flow arround a circular cylinder: A comparison with experimental visualization and measurements," J. Fluid Mech. **160**, 93–117 (1985).
[6]C.-C. Chang and R.-L. Chern, "A numerical study of flow around an impulsively started circular cylinder by a deterministic vortex method," J. Fluid Mech. **233**, 243–263 (1991).
[7]M.-H. Chou and W. Huang, "Numerical study of high-Reynolds-number flow past a bluff object," Int. J. Numer. Methods Fluids **23**, 711–732 (1996).
[8]Y. V. S. S. Sanyasiraju and V. Manjula, "Flow past an impulsively started circular cylinder using a higher-order semi compact scheme," Phys. Rev. E **72**, 1–10 (2005).
[9]J. C. Kalita and R. K. Ray, "A transformation-free HOC scheme for incompressible viscous flows past an impulsively started circular cylinder," J. Comput. Phys. **228**, 5207–5236 (2009).
[10]J. C. Kalita and S. Sen, "The biharmonic approach for unsteady flow past an impulsively started circular cylinder," Commun. Comput. Phys. **12**, 1163–1182 (2012).
[11]J. C. Kalita and S. Sen, "Unsteady separation leading to secondary and tertiary vortex dynamics: The sub-α- and sub-β-phenomena," J. Fluid Mech. **730**, 19–51 (2013).
[12]S. Sen, J. C. Kalita, and M. M. Gupta, "A robust implicit compact scheme for two-dimensional unsteady flows with a biharmonic stream function formulation," Comput. Fluids **84**, 141–163 (2013).
[13]T. Ma and S. Wang, "Topology of 2D incompressible flows and applications to geophysical fluid dynamics," Rev. R. Acad. Cien. Serie A. Mat. **96**, 447–459 (2002).
[14]M. Ghil, J. G. Liu, C. Wang, and S. Wang, "Boundary-layer separation and adverse pressure gradient for 2-D viscous incompressible flow," Physica D **197**, 149–173 (2004).
[15]M. Ghil, T. Ma, and S. Wang, "Structural bifurcation of 2-D nondivergent flows with Dirichlet boundary conditions applications to boundary-layer separation," SIAM J. Appl. Math. **65**, 1576–1596 (2005).
[16]A. V. Obabko and K. W. Cassel, "Navier-Stokes solutions of unsteady separation induced by a vortex," J. Fluid Mech. **465**, 99–130 (2002).
[17]A. V. Obabko and K. W. Cassel, "On the ejection-induced instability in Navier-Stokes solutions of unsteady separation," Philos. Trans. R. Soc., A **363**, 1189–1198 (2005).
[18]K. W. Cassel, F. T. Smith, and J. D. Walker, "The onset of instability in unsteady boundary-layer separation," J. Fluid Mech. **315**, 223–256 (1996).